

Phase formation and transition in a xanthan gum/H₂O/H₃PO₄ tertiary system

Syang-Peng Rwei · Tuan-Anh Nguyen

Received: 13 October 2013 / Accepted: 5 February 2014 / Published online: 16 February 2014
© Springer Science+Business Media Dordrecht 2014

Abstract Phase formation and transition in a xanthan gum (XG)/H₂O/H₃PO₄ tertiary system were characterized by polarized optical microscopy, light transmission detection and rheological methods. Three distinct phases and a transition region—the completely separated (S) phase, the liquid crystalline (LC) miscible phase, the isotropically (I) miscible phase and the S plus LC region—were identified. The presence of H₃PO₄ in the XG/H₂O system inhibited the evolution of both the S and LC phases. The S and LC phases contained less than 73 and 62 wt% of H₃PO₄, respectively. As the temperature increased over 65 °C, the LC phase in the H₃PO₄-rich and H₂O-poor region seriously shrunk owing to the breakup of hydrogen bonds among the XG helical structure. At the same XG loading, the viscosity of the XG solutions in LC phase was found to be much higher than that in I phase. It indicated the existence of numerous XG intermolecular interactions in the LC phase that suppress the movement of liquid. A study of the kinetics demonstrated that the shrinkage relaxation time (τ) depended strongly on temperature and was fitted by the Volgel-Fulcher-Tamman (VFT) expression. The potential energy barrier of this liquid was quite low at approximately 3.0 kJ mol⁻¹, falling in the

range of hydrogen-bond disassociation. The light absorbance test in heating mode revealed a biphasic transitional region between the LC phase and I phase. The contour of this region depended on the heating rate, and this fact was explained again by the relaxation behavior of XG helices at temperatures higher than 65 °C.

Keywords XG (xanthan gum) · XG/H₂O/H₃PO₄ tertiary system · Phase transition · Transitional region · Relaxation time

Introduction

Xanthan gum (XG) is one of the most important polysaccharides. It can increase the solution viscosity significantly with very little loading and therefore has been extensively used in many fields such as food processing, coatings, paper forming and oil recovery (Katzbauer 1998; Becker et al. 1998; Palaniraj and Jayaraman 2011). XG in aqueous solution exhibits not only excellent viscosity, but also liquid crystalline (LC) behavior with high stability in a wide range of concentrations (Milas et al. 1985; Iseki et al. 2001; Boyd et al. 2009). Owing to the helical and chiral structure of the XG molecule, such a cholesterol-LC characteristic has attracted the interest of scientists around the world. The stability of helices is believed to arise from non-covalent bonds, including hydrogen

S.-P. Rwei (✉) · T.-A. Nguyen
Institute of Organic and Polymeric Materials, National
Taipei University of Technology, #1, Sect. 3, Chung-
Hsiao E. Rd, Taipei, Taiwan, ROC
e-mail: f10714@ntut.edu.tw

bonding, electrostatic interactions and the steric effect (Li et al. 1999; Zuev et al. 2008). In general, the LC phase observed at a critical mesophase concentration in a XG/H₂O binary system is associated with the formation of a strand-like morphology, namely a rod-like conformation (Maret et al. 1981; Finkelmann and Schafheutle 1986; Lühmann and Finkelmann 1987; Allain et al. 1998; Boyd et al. 2009).

Many innovative techniques have been utilized to examine structural changes of XG polymer and its mixtures. To study the structure and deformation of single XG chains on the molecular scale, atomic force microscopy (AFM) has been widely applied to elucidate the architecture of complex or branched macromolecules (Gunning et al. 1995; Kirby et al. 1995; Gunning et al. 1996; Li et al. 1999; Iijima et al. 2007; Wu et al. 2009). Differential scanning calorimetry (DSC) has been used to determine the influence of H₂O content on the transition from the mesophase to isotropic phase and to provide comprehensive information on related changes in the oscillations of the network structure (Wiegeleben and Demus 1988; Yoshida et al. 1990; Quinn et al. 1994; Fujiwara et al. 2000; Raschip et al. 2008). Numerous authors have also noted that under certain conditions, the LC phase can be observed in XG aqueous solutions under a polarized light microscope owing to its particular texture (Maret et al. 1981; Yoshida et al. 1990; Allain et al. 1998; Dong et al. 2006). Light scattering techniques have been applied to investigate phenomena associated with the thermal motion of XG molecules, such as the thermal transition, mechanism of gel formation, critical overlap concentration, molecular diffusion and others (Southwick et al. 1979, 1981; Paradossi and Brant 1982; Covielo et al. 1987; Hacche et al. 1987; Berth et al. 1996).

Most studies in this field have focused on some essential characteristics of aqueous XG solution, especially structural features (Fujiwara et al. 2000; Bezemer et al. 1993), rheological properties (Xuewu et al. 1996; Lee and Brant 2002; Rinaudo and Moroni 2009; Choppe et al. 2010; Zhong et al. 2013) and thermal effects (Lambert and Rinaudo 1985). However, in the application of using XG as a thickener for oil recovery or other industrial applications, the rheological properties of the solution could be significantly affected by the presence of some acids such as H₃PO₄ or HCl. In this work, following the procedure of our previous study on the HPC/H₂O/H₃PO₄ tertiary

system (Rwei and Lyu 2012, 2013), XG aqueous solutions blended with various amounts of H₃PO₄ were investigated. This was useful to systematically evaluate the effects of compositional concentrations, temperature, annealing time and heating rate on the phase formation and transitions for the XG/H₂O/H₃PO₄ tertiary system. A kinetic model was proposed thereafter. Results of this study are useful in designing a temperature-sensitive thickener for the coating or oil recovery industry in the future.

Experiments

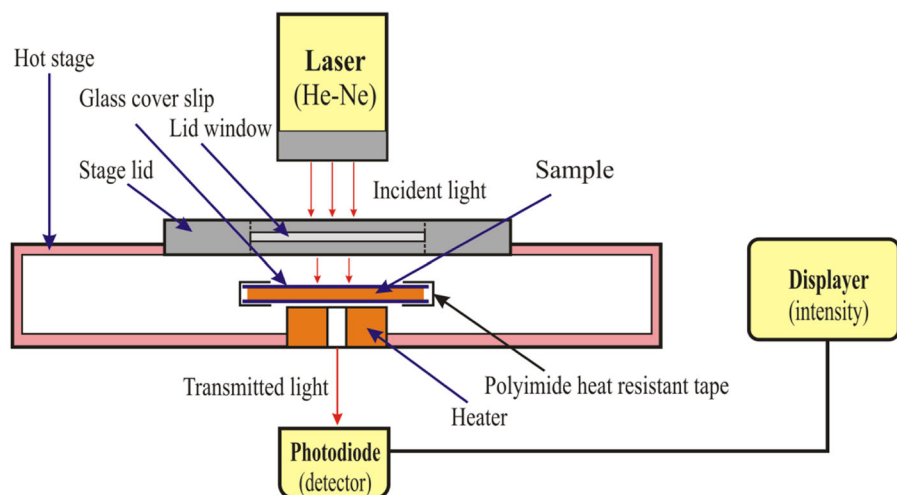
Materials

XG powder was purchased from Sigma-Aldrich (USA) without further purification. Phosphoric acids (pure and 85 wt%) were provided by Acros Organics (USA). Deionized water was used as a solvent and filtered through a reverse osmosis and deionizer system. Solutions were prepared by dissolving various concentrations of compositions at room temperature for 24 h before measurements were conducted. These samples were sealed and stored in a cabinet with controlled humidity (25 °C, 85 % RH) to inhibit the leakage of water. In the experiments, the concentration ranges of XG, deionized water and phosphoric acid were 4–70, 0–96 and 0–100 wt%, respectively. All solutions were stirred for more than 30 min with an rpm less than 60 to ensure the homogeneity of mixing without entrapping any bubble. In heating modes, the samples were placed between two microscope cover glasses (15 × 15 mm) and wrapped in heat-resistant polyimide tape provided by Chuan Chi Co., Ltd. (Taiwan), to prevent any change in the thickness and vaporization of water (Fig. 1). A phase diagram of the XG/H₂O/H₃PO₄ tertiary system in the temperature range from 25 to 95 °C was obtained.

Polarized optical microscope

Optical observations were made to elucidate the formation of phases using a polarized optical microscope (POM) from Nikkon (Labphoto2-Pol) that was assembled with a hot stage (HFS91) and a heat controller (TMS93) from Linkam. A beam of polarized light passed through and interacted with molecules in the liquid. The path lengths of the rod-like

Fig. 1 Experimental setup for measuring the transmitted light intensity including a hot stage and a light transmission detector



macromolecules varied with their orientations. Accordingly, the obtained wavelengths of the transmitted light were changed, producing various colors. The textural differences of POM images at various concentrations and temperatures proved the existence of distinct phases in the XG/H₂O/H₃PO₄ tertiary system.

Rheological measurements

The rheological measurements of concentrated solutions were made using a Physica MCR301 device with a PP25-SN12146 parallel plate (with a diameter of 24.5 mm and gap of 1 mm). The complex viscosity was obtained herein as plotting the viscosity versus frequency in a linear oscillation mode. The range of frequencies over which measurement was made at room temperature ran from 0.1 to 100 Hz. The viscosity, which quantifies the strength of intermolecular interactions, is known to be affected by both the concentration and temperature of the solution.

Transmission light detector

To determine the kinetics of the phase transition from LC to I phase, the absorbance of light is determined as a function of temperature using the method of light transmission detection. A laser beam was projected onto a sample, which was placed in a hot stage (HFS91). A photodiode was placed behind the hot stage to detect the intensity of the transmitted light through the samples (Fig. 1). The transmitted light by

samples was affected by temperature and the conformation of molecules. The change in absorbance with temperature at various annealing periods or heating rates yields information on structural deformation in the solution.

Results and discussion

Phase-formation thermodynamics: phase formation at room temperature

To construct a phase diagram of the XG/H₂O/H₃PO₄ tertiary system, over 80 points of the diagram were observed at room temperature. Figure 2 displays the textures of three distinct phases and a transition region at room temperature; these were the isotropically (I) miscible phase, the liquid crystalline (LC) miscible phase, the completely separated (S) phase and the LC plus S region. The variation in the color of a liquid results from the selective absorption and scattering of light. The features of particular LC samples in POM images yield information on the birefringence and anisotropic nature of the polysaccharide molecules. Based on the differences among LC samples, a phase diagram of the XG/H₂O/H₃PO₄ tertiary system, presented in Fig. 3, was obtained, in which the S, LC and I phases and the LC plus S region are shown in grey, yellow, white and pink, respectively.

In the XG–H₂O binary system, only three distinct phases were observed without a (S + LC) transition region. With regard to structural formation of

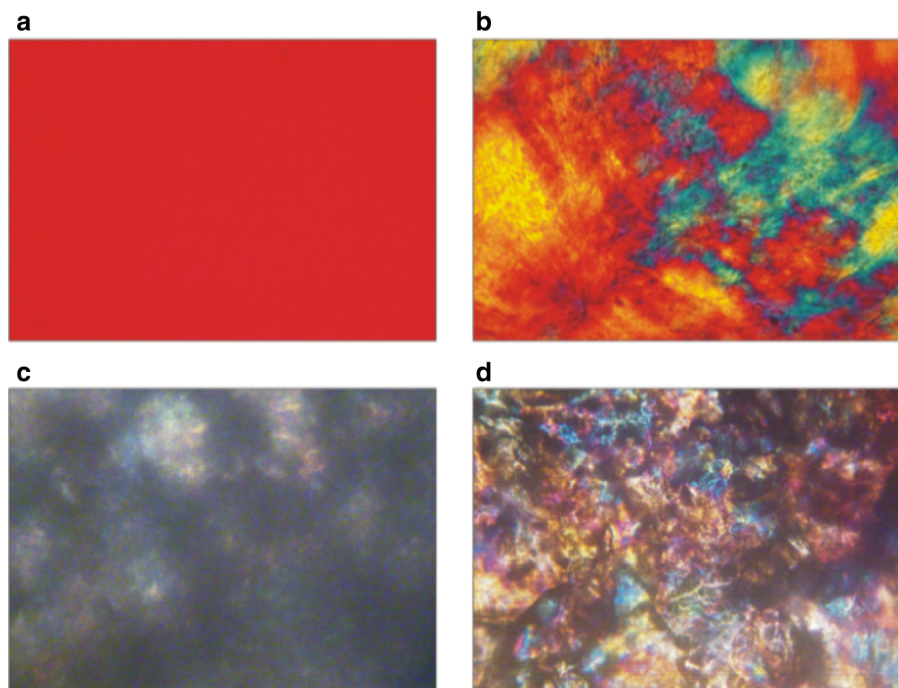


Fig. 2 Polarized optical microscope (POM) images exhibiting different phases of the XG/H₂O/H₃PO₄ tertiary system. **a** Isotropically (I) miscible phase, **b** liquid crystalline (LC) miscible phase, **c** completely separated (S) phase and **d** LC plus S region

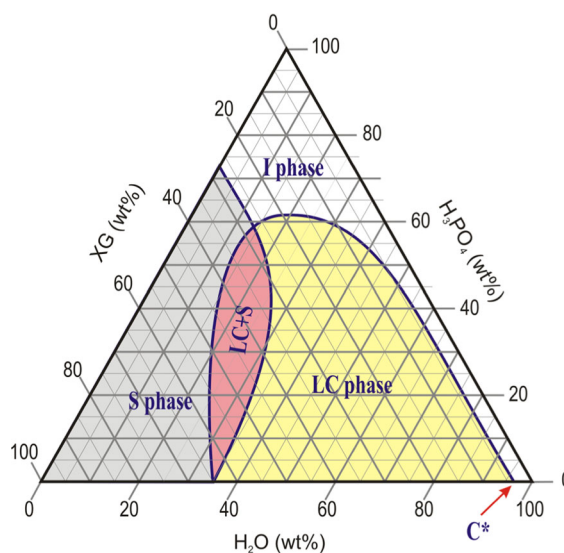


Fig. 3 Phase diagram of the XG/H₂O/H₃PO₄ tertiary system at room temperature

polysaccharides in concentrated solution, it is known that the separation from mesophase to isotropic phase reduces repulsive interactions and the association between macromolecules depends on the abundance of hydroxyl groups (Burchard 2001). Furthermore, the

content of H₂O in the system is the determinant of the appearances of both the glassy phase and the LC phase (Yoshida et al. 1990). The hydrogen bonds, which are generated between the H₂O and the hydroxyl groups of the XG molecules, play an important role in the formation of a mesophase because of their highly conformational stability. The LC phase in the XG/H₂O binary system was exhibited in a quite wide range of XG concentrations from 4 to 66 wt%.

The mesophase was not found in the phase diagram of the XG/H₃PO₄ binary system since the required intermolecular interactions were absent. The rod-like helices in the system did not adopt a particular orientation or orientation distribution with respect to each other, as did the liquid crystals in the XG/H₂O binary system. Simply, the critical XG concentration at which the miscibility of the mixture reached its maximum value was around 27 wt%. At lower concentrations, XG was fully dissolved in H₃PO₄ solvent in a disordered manner or an isotropic phase. Moreover, the acid hydrolysis may have substantially shortened the backbones of XG to an extent that depended on the H₃PO₄ content of the solutions (Christensen et al. 1993).

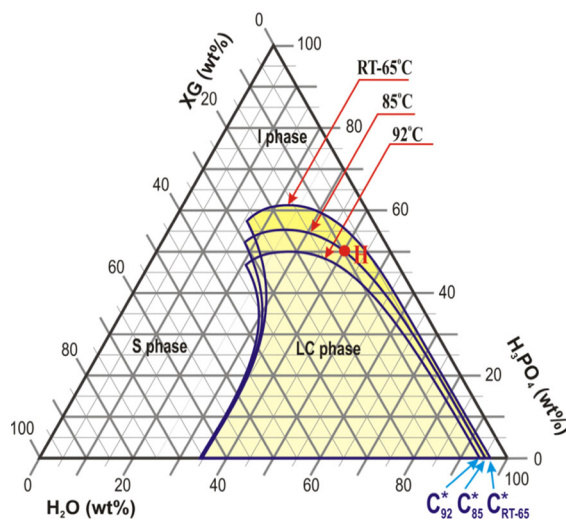


Fig. 4 Evolution of LC phase after annealing at 85 and 92 °C for 60 min

Based on the above discussion, the XG/H₂O/H₃PO₄ tertiary system was established by adding H₃PO₄ to the XG/H₂O binary system. The formation of distinct phases, as shown in Fig. 3, can be understood by combining the two phase diagrams above. Some interesting results can be deduced from the evolution of the phase diagram. First, the partial formation of the LC phase revealed that the lyotropic characteristic of XG/H₂O/H₃PO₄ solutions could be diminished to an extent that depended on the quantity of H₃PO₄ therein. Adding H₃PO₄ to the system shrunk the LC and S phases and enlarged the I phase. The presence of H₃PO₄ not only decreased the miscibility of XG in aqueous solution, but also suppressed the evolution of LC behavior. Notably, the S and LC phases contained less than 73 and 62 wt% of H₃PO₄, respectively.

The critical XG mesophase concentration C* shown in Fig. 4 was used to determine the boundary between the LC phase and I phase (Allain et al. 1998; Dong et al. 2006). Clearly, the planar texture in the concentrated solution was characteristic of the cholesteric LC phase because the axes of the spirals were almost perpendicular to the sample plane (Fig. 2b). C* was retained at H₃PO₄ concentrations lower than 45 wt%, but its amount rapidly increased with increasing H₃PO₄ content up to 62 wt%, at which concentration the LC phase became extinct at room temperature. The threshold C* at this point with maximum H₃PO₄ content was 19 wt%, indicating that the dramatic collapse of intermolecular attraction by

H₃PO₄ was responsible for the elimination of the LC domain. The sharp increase in C* was caused by the excessive addition of H₃PO₄ to aqueous XG. The stability of LC solutions in the H₂O-rich and H₃PO₄-poor region arises from the inhibition of impregnation of H₃PO₄ by a stationary configuration of XG helices with the majority of intermolecular interactions, such as hydrogen bonds. If another weaker acid is applied herein to replace H₃PO₄, the maximum acid loading will be higher than 62 wt% because of less inhibition effect. More investigations to confirm this point are being carried out, and the results will be published in the near future.

Effect of temperature on phase formation

The above procedure at various temperatures revealed the evolution of the phase diagram from room temperature to 92 °C, as displayed in Fig. 4. Interestingly, the overall phase diagram changed very little from room temperature to 65 °C, mainly owing to the upper critical solution temperature (UCST) behavior of the XG solution rather than the lower critical solution temperature (LCST) behavior that is exhibited by numerous polysaccharides (Cowie and Arrighi 2001). However, once the temperature rises over 65 °C, a slow phase transition occurs. As an example at point H, the phase transition at 85 °C was not detected in the initial stage of the heating process because the thermal relaxation behavior of XG helices was difficult to approach immediately. Nevertheless, after about 60 min of annealing, a textural difference or phase transformation was observed in the H₃PO₄-rich region, but not in the H₂O-rich region. Figure 4 shows that the LC phase behaved with severe shrinkage in the H₃PO₄-rich region but a slight enlargement in the XG-rich region as the temperature was increased from 65 to 92 °C for 60 min of annealing time. This indicates that the increase in temperature reduced the maximum loading of H₃PO₄ but slightly increased that of XG in the LC boundary line. As noted previously, the change in C* was caused by the addition of H₃PO₄ to the XG solution. Notably, adding H₃PO₄ to XG/H₂O would considerably increase the gradient of C* with respect to temperature. The evolutions of the S and S plus LC regions were also strongly affected by temperature in the H₃PO₄-rich region, as presented in Fig. 5. The solubility of XG in the S phase increased remarkably with temperature by the promotion of acid

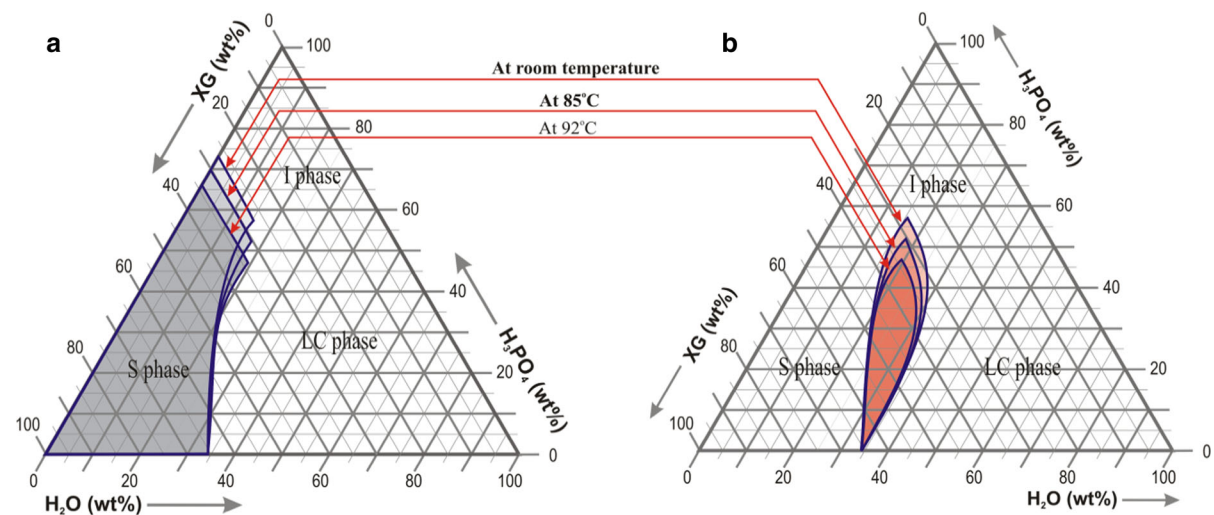


Fig. 5 Evolution of S phase and S plus LC region annealed at 85 and 92 °C for 60 min

hydrolysis and acceleration of molecular motion. Weak interactions among molecules were further eliminated when heat energy was provided, forming a more homogeneous solution with a more random arrangement. In the S plus LC region, the dispersion and uniformity of XG molecules in the solvents increased with temperature. Thus, the top of this transition region, in which XG-poor but H_3PO_4 -rich solutions possessed very weak interactions, shrunk considerably as the temperature increased. Moreover, the present authors recently found that temperature had no effect on the miscibility of the blended system that contained more than 45 wt% of XG (Basvaraju et al. 2007). The phase diagram of the XG/ H_2O system herein shows no change from the S plus LC region to the S phase with temperature.

Rheological measurement of the effect of frequency on phase transition

Figure 6 indicates that the viscosity at points M_1 , M_2 and M_3 in the LC phase was much higher than that at point M_4 in the I phase at the same XG loading, revealing the presence of numerous intermolecular hydrogen bonds in the LC phase, which suppress liquid movement. Furthermore, Fig. 6 reveals a very slight difference in viscosity and a similar slope of the viscosity-thinning plots among the M_1 , M_2 and M_3 points, whose acid content varied but XG concentration remained the same (10 wt%). This result indicates

that the acid concentration has little effect on the fluid behavior as long as the XG solutions stay within the LC region. In general, oriented rod-like molecules, without any functional groups pendant to their surfaces, exhibit LC behavior with a low viscosity. However, the high regularity of XG molecules in the LC phase easily induced the formation of intermolecular rather than intramolecular hydrogen bonds among numerous pendant hydroxyl groups of the XG helices. The fluidity of the LC phase therefore was significantly reduced. In short, our viscosity measurements confirm the existence of some intermolecular hydrogen bonds in the LC phase.

Phase-formation kinetics: effect of isothermal annealing time on phase formation

The evolution of the LC phase at 85 °C is shown in Fig. 7, demonstrating the existence of a transitional region before a thermal equilibrium. This region formed because, when the temperature exceeds 65 °C, the hydrogen bonds are broken and other interactions eliminated, loosening the structure of the LC solutions. However, the relaxation of XG molecules in the structural transformation, from the LC state to a more disordered state, takes time. A long annealing period is therefore required for molecular relaxation, and this can be recorded as the relaxation time at the given lower temperature. Additionally, at a higher temperature, such as 92 °C, more hydrogen and non-covalent

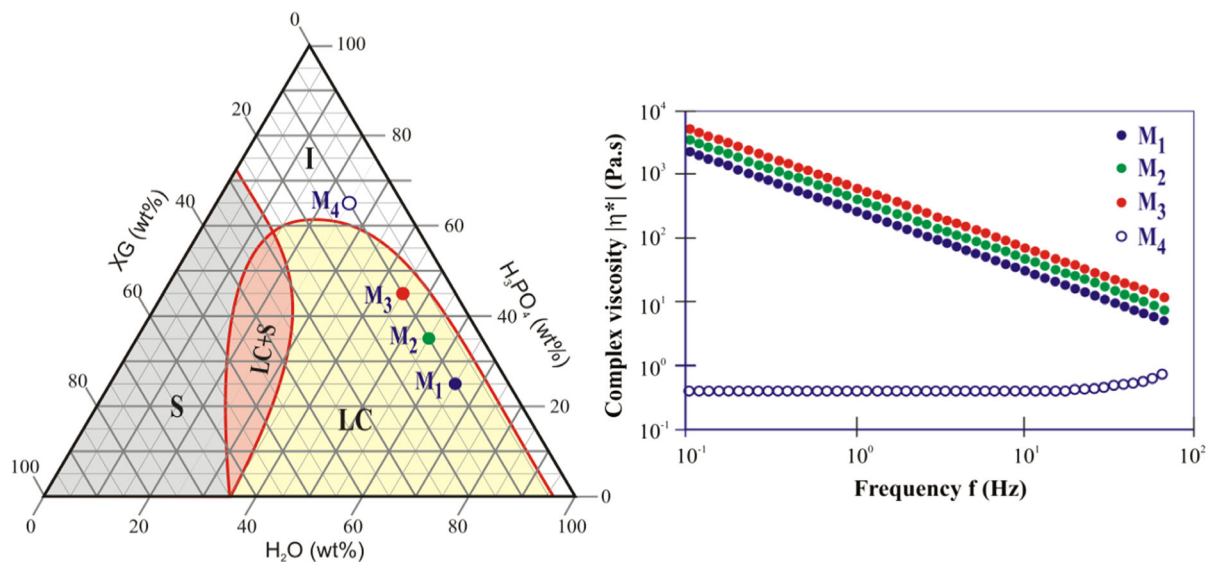


Fig. 6 Effect of frequency on phase transition obtained at various H_3PO_4 concentrations

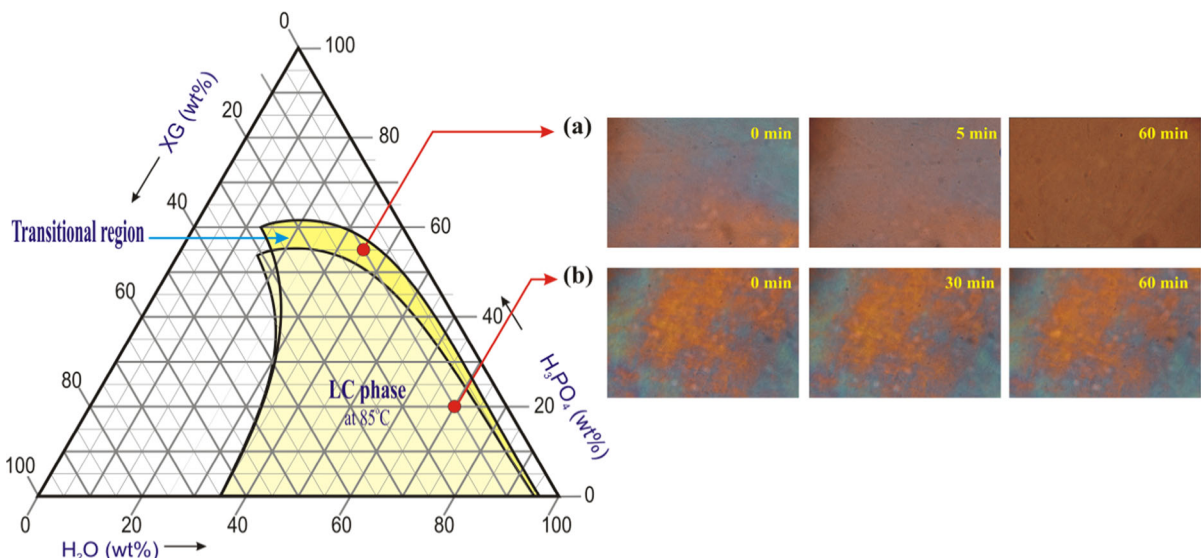


Fig. 7 Temperature and annealing time dependence of LC solutions at the same XG concentration investigated in **a** the transitional region (non-equilibrium state) and **b** the stable region of the LC phase after annealing at 85 °C for 60 min

interactions among LC molecules are thermally disrupted, forming an isotropic state in which the molecules exhibit random-walk behavior. The transition is relatively easy, and the required annealing time is short. Figure 8 plots annealing time as a function of phase transition temperature at a specific LC point, H ($\text{XG}/\text{H}_2\text{O}/\text{H}_3\text{PO}_4:10/40/50$ wt%), marked in the transition region in Fig. 4. A previous investigation reported that at a given temperature, disentanglements

among the noncrystalline region and breakup of hydrogen bond among the helical region of XG molecules would gradually proceeded in the course of annealing (Iseki et al. 2001). The annealing time, which is related to the relaxation time of the XG molecules, is a function of the phase transition temperature. Figure 8 indicates that a phase transition occurred in the LC solution ($\text{XG}/\text{H}_2\text{O}/\text{H}_3\text{PO}_4:10/40/50$ wt%) annealed at 85 °C for at least 55 min.

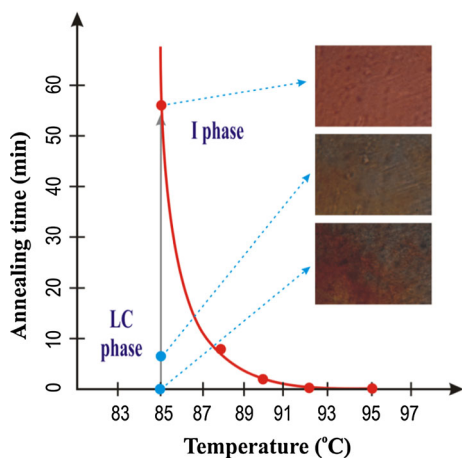


Fig. 8 Dependence of the phase transition temperature on annealing time observed at point H ($\text{XG}/\text{H}_2\text{O}/\text{H}_3\text{PO}_4:10/40/50$ wt%, referring to Fig. 4) in the transitional region

However, when it was annealed at 90 °C, the phase transition time was reduced to as short as 3 min.

The relationship between phase transition temperature and annealing time followed as a non-linear function that was similar to a hyperbola. For a liquid, the temperature dependence of structural relaxation time (τ) is given by the Volgel-Fulcher-Tamman (VFT) expression for phase transition kinetics, as follows (Dyre 1998; Rault 2000; Ikeda and Aniya 2013).

$$\tau = \tau_0 \exp\left(\frac{E}{R(T - T_0)}\right) \quad (1)$$

$$\ln \tau = \ln \tau_0 + \frac{E}{R} \left(\frac{1}{T - T_0} \right) \quad (2)$$

where τ_0 is a pre-exponential factor, E is the activation energy, T_0 is the reference temperature at which there is no excluded volume (65 °C or 338 K in the XG system herein), and R is the universal gas constant.

Figure 9 plots the linear relationship between $\ln \tau$ and $1/(T - T_0)$ at point H on a diagram with a specific slope suggesting that the structural relaxation time is an exponential function of temperature. According to Eqs. (1) and (2), the activation energy for the dissociation of molecules can be calculated from the slope of the plot (E/R). Clearly, the potential energy barrier of this liquid is only about 3.0 kJ mol⁻¹, which is much lower than the energies of other bonds such as covalent bonds (30–100 kJ mol⁻¹). This finding shows that most of the interactions that are eliminated

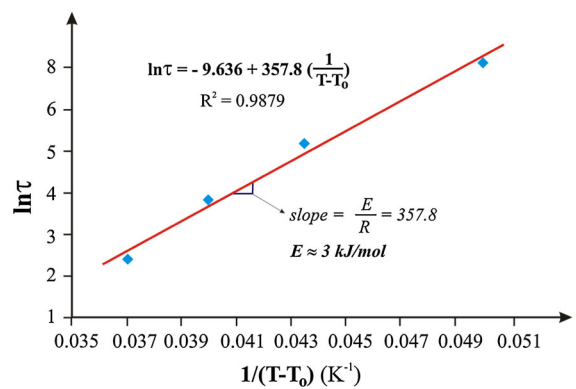


Fig. 9 Plot of $\ln \tau$ against $1/(T - T_0)$ for point H (refer to Fig. 4) showed the temperature dependence of relaxation time

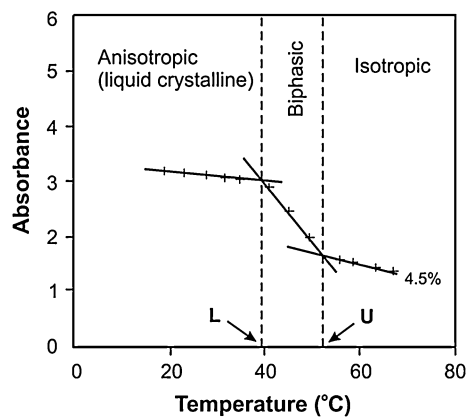


Fig. 10 Change in optical absorbance against temperature clarified the appearance of phase transition for LC polysaccharide solutions. These experimental results were investigated at 4.5 wt% of levan in aqueous solution (Huber et al. 1994)

by heat are not as strong as chemical bonds and so must be hydrogen bonds. Hence, the provision of sufficient heat within a certain period can activate the dissociation of intermolecular interaction or chain entanglement in a H_3PO_4 -rich LC state, and an isotropic state can finally be reached.

Effect of heating rate on phase transition, as determined by light absorbance test

When a beam of incident light strikes a solution, it divides into scattered, absorbed and transmitted light. In most cases of oriented light, the intensity of transmitted radiation (I) is less than that of incident radiation (I_0) because some light is absorbed and some is scattered. As stated in the Beer-Lambert law,

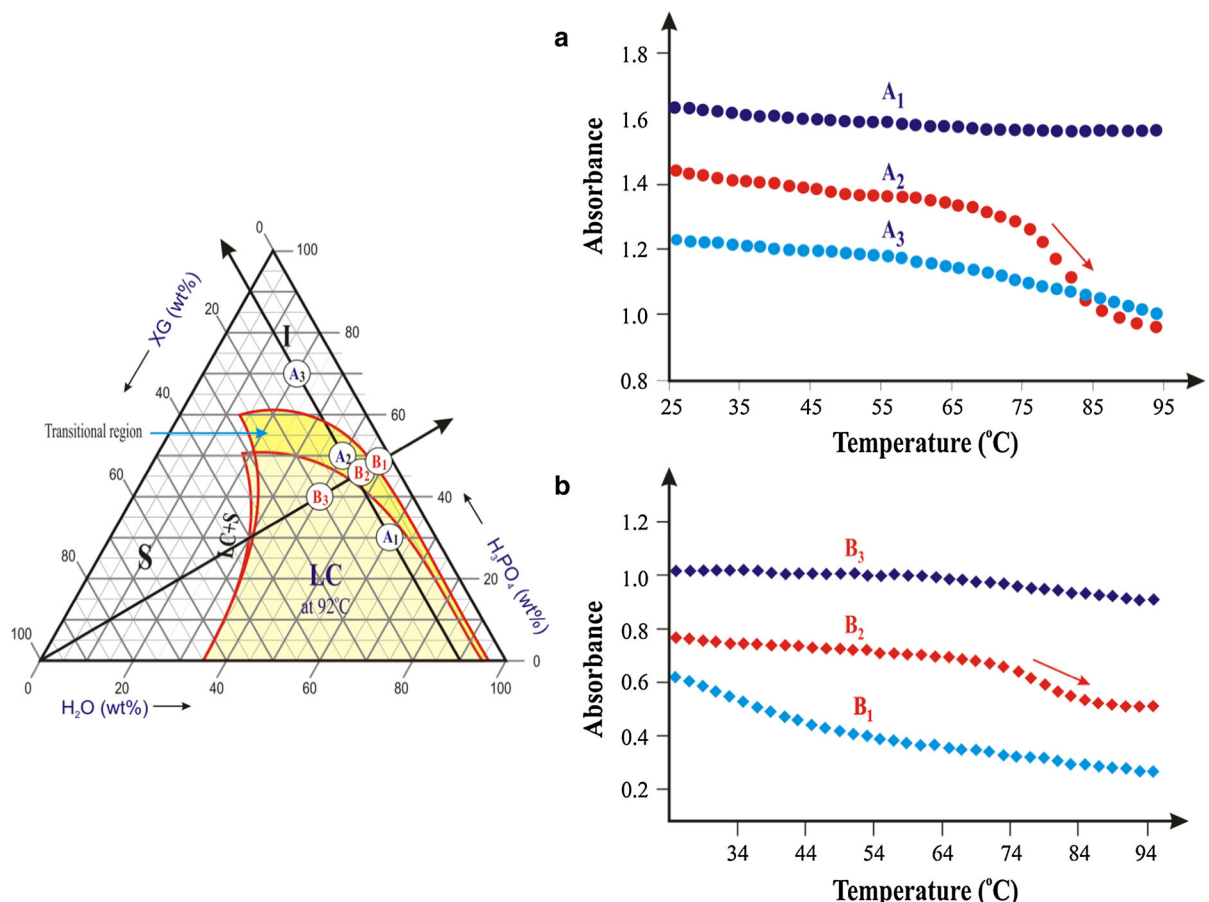


Fig. 11 Effect of compositional concentrations on phase transition through the plots of absorbance against temperature measured at a 10 wt% of XG with 30, 50 and 70 wt% of H_3PO_4 and **b** the same ratio of solvents ($H_2O:H_3PO_4 = 1:1$) with 3, 7 and 20 wt% of XG

absorbance (α), also called optical density, is directly proportional to the concentration of the sample:

$$\alpha = \ln\left(\frac{I_o}{I}\right) \quad (3)$$

Huber et al. (1994) studied the phase transition of aqueous solutions of levan (a polysaccharide) by cooling them in water baths. He found that the absorbance of such a solution at a given wavelength was a function of temperature. The lower (L) and upper (U) temperatures, presented in Fig. 10, indicate a range in which turbidity changes most rapidly owing to the deformation and consequent change in the volume fraction of LC samples. The appearance of a biphasic region between L and U arises from the destruction of XG molecules at elevated temperatures.

In this kinetic study, experiments were carried out in which heating resulted in a change in optical

absorbance with temperature, reflecting the conformational variation of XG helices. As shown in Fig. 11, the structures of LC samples changed suddenly in the transitional region, but not in other regions. Therefore, the following conclusions were drawn.

First, for samples A₂ and B₂, the orientation of liquid crystals in solution varied considerably as the temperature increased, since the heat energy separated the XG helices from each other. Most intermolecular bonds, such as hydrogen bonds, were rapidly broken, and a disordered structure of randomly oriented coils was formed.

Second, as discussed above, the formation of a transitional region was caused by the H_3PO_4 in XG aqueous solution as the temporary bonds formed between molecules; this region shrank as the temperature increased. Figure 11a reveals that as more H_3PO_4 was added, less light was absorbed, resulting

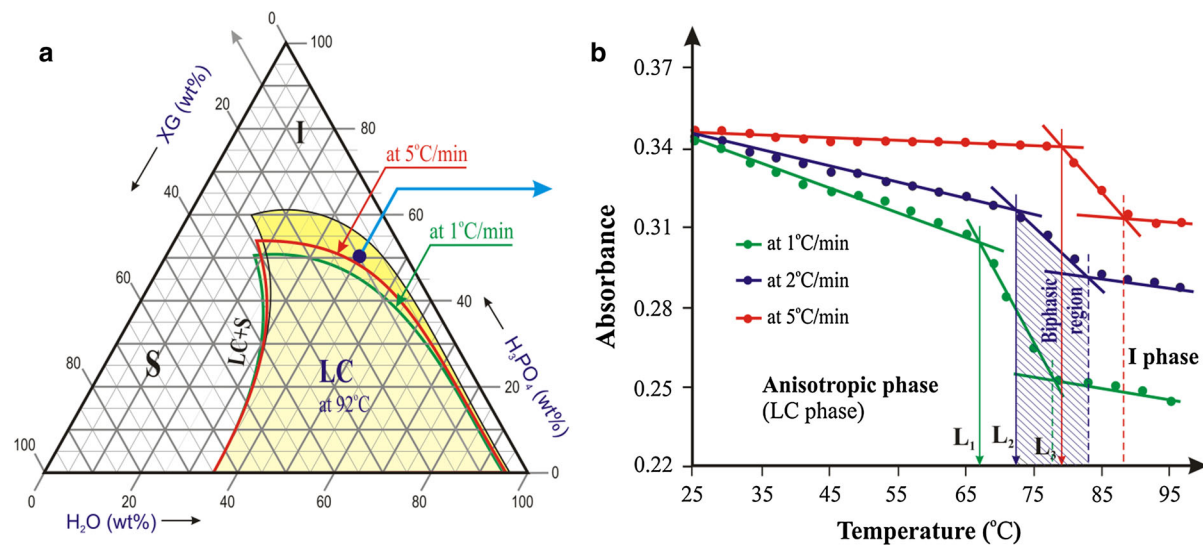


Fig. 12 Dependence of phase transition on the heating rate presented on **a** the phase diagram of the tertiary system at 92 °C and **b** the plots of absorbance versus temperature for an LC

solution (XG/H₂O/H₃PO₄: 10/40/50 wt%) in the transitional region at 1, 2 and 5 °C/min

in the low turbidity of the samples in the H₃PO₄-rich region. The slight change in absorbance of samples A₁ or A₃ with temperature was related to the saturation of interactions. The decrease in absorbance in the isotropic region (A₃) was affected by the acid hydrolysis of XG molecules, whereas that in the H₂O-rich LC region (A₁) was clearly related to the maintenance of the structure by numerous hydrogen bonds. Notably, point A₂ shows an abrupt decrease due to experiencing the transition state from LC phase to I phase as the temperature increases.

Finally, Fig. 11b shows the effect of XG concentration on the formation of the LC phase. The absorbance of sample B₁, which is barely below the critical concentration of the LC formation, was much lower than that of samples B₂ and B₃, where the turbidity increased significantly because the XG concentration passed over the LC threshold. Once a lyotropic LC phase was formed, increasing XG concentration would increase the compact density of helices, stabilize the LC structure in solution and screen out the light. Moreover, similar to point A₂ shown above, the transitional point B₂ in Fig. 11b exhibits an abrupt decrease. These results are consistent with earlier observations for the effects of constitution concentrations on phase formation.

As mentioned before, the breakup of intermolecular hydrogen bonds among the helices of the XG polysaccharides is responsible for the thermal

relaxation behavior. To further understand the transition kinetics, the measurements of optical absorbance at various heating rates were made. Figure 12a shows that the equilibrium LC phase was not achieved when the heating was too fast. For instance, at a temperature of 92 °C, the shrinkage of the LC phase that was obtained at 5 °C/min was less than that obtained at 1 °C/min. The thermal equilibrium state could be approached at lower heating rates and consequently longer transition time.

Figure 12b plots the effect of the heating rate on absorbance for the LC sample (XG/H₂O/H₃PO₄: 10/40/50 wt%) in the temperature-transition region. Notably, the plots of absorbance versus temperature were revealed to specify different biphasic regions at various heating rates. The initial points L that were determined at heating rates of 1, 2 and 5 °C/min were 67, 72 and 79 °C, respectively. Reducing the rate of heating decreased both the phase transition temperature and the optical absorbance. An LC solution should be in thermal equilibrium at a lower temperature when it is heated more slowly.

Conclusions

In this work, phase formation and transition of the XG/H₂O/H₃PO₄ tertiary system were determined by polarized optical microscopy, light transmission detection

and rheological measurements. Three distinct phases and a transition region—the S phase, LC phase, I phase and S plus LC region—were identified. The presence of H_3PO_4 in the XG/ H_2O system inhibited the evolution of both the S and LC phases. As the temperature increased over 65 °C, a serious shrinkage of the LC phase took place in the H_3PO_4 -rich but H_2O -poor region. This was due to the breakup of hydrogen bonds among XG helical structures. The viscosity of the LC phase was much higher than that of the I phase at the same XG loading, indicating the existence of numerous intermolecular hydrogen bonds in the LC phase to suppress the liquid movement. The kinetic study revealed that the shrinkage relaxation time (τ) strongly depends on temperature and can be fitted by the Vogel–Fulcher–Tammann (VFT) expression. The potential energy barrier of this liquid is quite low at about 3.0 kJ mol^{−1}, falling in the range of hydrogen-bond disassociation. The light absorbance test in a heating mode reveals that a biphasic transitional region from LC to I phase was observed. The area of this region showed a dependence on the heating rate and can be explained again by the relaxation behavior of XG helices at elevated temperatures.

Acknowledgments The authors would like to thank the National Science Council of the Republic of China, Taiwan, for financially supporting this research under contract no. NSC 102-2221-E-027-110-MY3. Ted Knoy is appreciated for his editorial assistance.

References

- Allain C, Lecourtier J, Chauveteau G (1998) Mesophase formation in high molecular-weight xanthan solutions. *Rheol Acta* 27(3):255–262. doi:[10.1007/BF01329741](https://doi.org/10.1007/BF01329741)
- Basavaraju KC, Demappa T, Rai SK (2007) Miscibility studies of polysaccharide xanthan gum and PEO (polyethylene oxide) in dilute solution. *Carbohydr Polym* 69:462–466
- Becker A, Katzen F, Puhler A, Ielpi L (1998) Xanthan gum biosynthesis and application: a biochemical/genetic perspective. *Appl Microbiol Biotechnol* 50(2):145–152. doi:[10.1007/s002530051269](https://doi.org/10.1007/s002530051269)
- Berth G, Dautzenberg H, Christensen BE, Harding SE, Rother G, Smidsrød O (1996) Static light scattering studies on xanthan in aqueous solutions. *Macromolecules* 29(10):3491–3498. doi:[10.1021/ma9515386](https://doi.org/10.1021/ma9515386)
- Bezemer L, Ubbink JB, Kooker JAD, Kuil ME, Leyte JC (1993) On the conformational transitions of native xanthan. *Macromolecules* 26(24):6436–6446. doi:[10.1021/ma00076a021](https://doi.org/10.1021/ma00076a021)
- Boyd MJ, Hampson FC, Jolliffe IG, Dettmar PW, Mitchell JR, Melia CD (2009) Strand-like phase separation in mixtures of xanthan gum with anionic polyelectrolytes. *Food Hydrocoll* 23:2458–2467. doi:[10.1016/j.foodhyd.2009.07.008](https://doi.org/10.1016/j.foodhyd.2009.07.008)
- Burchard W (2001) Structure formation by polysaccharides in concentrated solution. *Biomacromolecules* 2(2):342–353. doi:[10.1021/bm0001291](https://doi.org/10.1021/bm0001291)
- Choppe E, Puaud F, Nicolai T, Benyahia L (2010) Rheology of xanthan solutions as a function of temperature, concentration and ionic strength. *Carbohydr Polym* 82(4):1228–1235. doi:[10.1016/j.carbpol.2010.06.056](https://doi.org/10.1016/j.carbpol.2010.06.056)
- Christensen BE, Smidsrød O, Elgsaeter A, Stokke BT (1993) Depolymerization of double-stranded xanthan by acid hydrolysis: characterization of partially degraded double strands and single-stranded oligomers released from the ordered structures. *Macromolecules* 26(22):6111–6120. doi:[10.1021/ma00074a037](https://doi.org/10.1021/ma00074a037)
- Coviello T, Burchard W, Dentini M, Crescenzi V (1987) Solution properties of xanthan—dynamic and static light scattering from semidilute solution. *Macromolecules* 20(5):1102–1107. doi:[10.1021/ma00171a038](https://doi.org/10.1021/ma00171a038)
- Cowie JMG, Arrighi V (2001) Polymers: chemistry and physics of modern materials, 2nd edn. CRC Press, Edinburgh
- Dong YM, Mao W, Wang HW, Zhao YQ, Li XJ, Bi DX, Yang LL, Ge Q, Fang XM (2006) Measurement of critical concentration for mesophase formation of chitosan derivatives in both aqueous and organic solutions. *Polym Int* 55(12):1444–1449. doi:[10.1002/pi.2099](https://doi.org/10.1002/pi.2099)
- Dyre JC (1998) Source of non-arrhenius average relaxation time in glass-forming liquids. *J Non Cryst Solids* 235–237:142–149
- Finkelmann H, Schafheutle MA (1986) Lyotropic liquid crystalline phase behaviour of a monomeric and a polymeric monosaccharide amphiphile in aqueous solution. *Colloid Polym Sci* 264(9):786–790. doi:[10.1007/BF01500754](https://doi.org/10.1007/BF01500754)
- Fujiiwara J, Iwanami T, Takahashi M, Tanaka R, Hatakeyama T, Hatakeyama H (2000) Structural change of xanthan gum association in aqueous solutions. *Thermochim Acta* 352–353(3):241–246. doi:[10.1016/S0040-6031\(99\)00472-4](https://doi.org/10.1016/S0040-6031(99)00472-4)
- Gunning AP, Kirby AR, Morris VJ, Wells B, Brooker BE (1995) Imaging bacterial polysaccharides by AFM. *Polym Bull* 34(5–6):615–619. doi:[10.1007/BF00423359](https://doi.org/10.1007/BF00423359)
- Gunning AP, Kirby AR, Morris VJ (1996) Imaging xanthan gum in air by ac “tapping” mode atomic force microscopy. *Ultramicroscopy* 63(1):1–3. doi:[10.1016/0304-3991\(96\)00032-0](https://doi.org/10.1016/0304-3991(96)00032-0)
- Hacche LS, Washington GE, Brant DA (1987) Light-scattering investigation of the temperature-driven conformation change in xanthan. *Macromolecules* 20(9):2179–2181. doi:[10.1021/ma00175a023](https://doi.org/10.1021/ma00175a023)
- Huber AE, Stayton SP, Viney C, Kaplan DL (1994) Liquid crystallinity of a biological polysaccharide: the levan/water phase diagram. *Macromolecules* 27:953–957
- Iijima M, Shinozaki M, Hatakeyama T, Takahashi M, Hatakeyama H (2007) AFM studies on gelation mechanism of xanthan gum hydrogels. *Carbohydr Polym* 68(4):701–707. doi:[10.1016/j.carbpol.2006.08.004](https://doi.org/10.1016/j.carbpol.2006.08.004)
- Ikeda M, Aniya M (2013) Understanding the Vogel–Fulcher–Tammann law in terms of the bond strength-coordination number fluctuation model. *J Non Cryst Solids* 371–372:53–57

- Iseki T, Takahashi M, Hattori H, Hatakeyama T, Hatakeyama H (2001) Viscoelastic properties of xanthan gum hydrogels annealed in the sol state. *Food Hydrocoll* 15(4–6):503–506. doi:[10.1016/S0268-005X\(01\)00088-1](https://doi.org/10.1016/S0268-005X(01)00088-1)
- Katzbauer B (1998) Properties and applications of xanthan gum. *Polym Degrad Stabil* 59(1–3):81–84. doi:[10.1016/S0141-3910\(97\)00180-8](https://doi.org/10.1016/S0141-3910(97)00180-8)
- Kirby AR, Gunning AP, Morris VJ (1995) Imaging xanthan gum by atomic force microscopy. *Carbohydr Res* 267(1):161–166. doi:[10.1016/0008-6215\(94\)00294-P](https://doi.org/10.1016/0008-6215(94)00294-P)
- Lambert F, Rinaudo M (1985) On the thermal stability of xanthan gum. *Polymer* 26:1549–1553. doi:[10.1016/0032-3861\(85\)90092-8](https://doi.org/10.1016/0032-3861(85)90092-8)
- Lee HC, Brant DA (2002) Rheology of concentrated isotropic and anisotropic xanthan solutions. 2. A semiflexible wormlike intermediate molecular weight sample. *Macromolecules* 35(6):2223–2234. doi:[10.1021/ma011527e](https://doi.org/10.1021/ma011527e)
- Li H, Rief M, Oesterhelt F, Gaub HE (1999) Force spectroscopy on single xanthan molecules. *Appl Phys A Mater* 68:407–410. doi:[10.1007/s003399900920](https://doi.org/10.1007/s003399900920)
- Lüthmann B, Finkelmann H (1987) Lyotropic liquid crystalline phase behavior of amphiphilic monomers and polymers having a rod-like hydrophobic moiety. *Colloid Polym Sci* 265(6):506–511. doi:[10.1007/BF01412504](https://doi.org/10.1007/BF01412504)
- Maret G, Milas M, Rinaudo M (1981) Cholesteric order in aqueous solutions of the polysaccharide xanthan. *Polym Bull* 4(5):291–297. doi:[10.1007/BF00255106](https://doi.org/10.1007/BF00255106)
- Milas M, Rinaudo M, Tinland B (1985) The viscosity dependence on concentration, molecular weight and shear rate of xanthan solutions. *Polym Bull* 14(2):157–164. doi:[10.1007/BF00708475](https://doi.org/10.1007/BF00708475)
- Palaniraj A, Jayaraman V (2011) Production, recovery and applications of xanthan gum by xanthomonas campestris. *J Food Eng* 106:1–12. doi:[10.1016/j.jfoodeng.2011.03.035](https://doi.org/10.1016/j.jfoodeng.2011.03.035)
- Paradossi G, Brant DA (1982) Light scattering study of a series of xanthan fractions in aqueous solution. *Macromolecules* 15(3):874–879. doi:[10.1021/ma00231a035](https://doi.org/10.1021/ma00231a035)
- Quinn FX, Hatakeyama T, Takahashi M, Hatakeyama H (1994) The effect of annealing on the conformational properties of xanthan hydrogels. *Polymer* 35(6):1248–1252. doi:[10.1016/0032-3861\(94\)90019-1](https://doi.org/10.1016/0032-3861(94)90019-1)
- Raschip IE, Yakimets I, Martin CP, Paes SS, Vasile C, Mitchell JR (2008) Effect of water content on thermal and dynamic mechanical properties of xanthan powder—a comparison between standard and novel techniques. *Powder Technol* 182(3):436–443. doi:[10.1016/j.powtec.2007.07.010](https://doi.org/10.1016/j.powtec.2007.07.010)
- Rault J (2000) Origin of the Vogel–Fulcher–Tammann law in glass-forming materials: the α - β bifurcation. *J Non Cryst Solids* 271:177–217
- Rinaudo M, Moroni A (2009) Rheological behavior of binary and ternary mixtures of polysaccharides in aqueous medium. *Food Hydrocoll* 23(7):1720–1728. doi:[10.1016/j.foodhyd.2009.01.012](https://doi.org/10.1016/j.foodhyd.2009.01.012)
- Rwei SP, Lyu MS (2012) 3-D phase diagram of HPC/H₂O/H₃PO₄ tertiary system. *Cellulose* 19(4):1065–1074. doi:[10.1007/s10570-012-9707-3](https://doi.org/10.1007/s10570-012-9707-3)
- Rwei SP, Lyu MS (2013) HPC/H₂O/H₃PO₄ tertiary system: a rheological study. *Cellulose* 20(1):135–147. doi:[10.1007/s10570-012-9810-5](https://doi.org/10.1007/s10570-012-9810-5)
- Southwick JG, McDonnell ME, Jamieson AM (1979) Solution studies of xanthan gum employing quasielastic light scattering. *Macromolecules* 12(2):305–311. doi:[10.1021/ma60068a029](https://doi.org/10.1021/ma60068a029)
- Southwick JG, Jamieson AM, Blackwell J (1981) Quasi-elastic light scattering studies of semidilute xanthan solutions. *Macromolecules* 14(6):1728–1832. doi:[10.1021/ma50007a022](https://doi.org/10.1021/ma50007a022)
- Wiegeleben A, Demus D (1988) Methodical aspects in thermal analysis of liquid crystalline substances. *J Therm Anal Calorim* 33(4):1207–1211. doi:[10.1007/BF01912751](https://doi.org/10.1007/BF01912751)
- Wu J, Deng X, Zhang Y, Wang L, Tian BQ, Xie BJ (2009) Application of atomic force microscopy in the study of polysaccharide. *Agric Sci China* 8(12):1458–1465. doi:[10.1016/S1671-2927\(08\)60359-4](https://doi.org/10.1016/S1671-2927(08)60359-4)
- Xuewu Z, Xin L, Dexiang G, Wei Z, Tong X, Yonghong M (1996) Rheological models for xanthan gum. *J Food Eng* 27(2):203–209. doi:[10.1016/0260-8774\(94\)00092-1](https://doi.org/10.1016/0260-8774(94)00092-1)
- Yoshida H, Hatakeyama T, Hatakeyama H (1990) Phase transitions of the water-xanthan system. *Polymer* 31(4):693–698. doi:[10.1016/0032-3861\(90\)90291-6](https://doi.org/10.1016/0032-3861(90)90291-6)
- Zhong L, Oostrom M, Truem MJ, Vermeul VR, Szecsody JE (2013) Rheological behavior of xanthan gum solution related to shear thinning fluid delivery for subsurface remediation. *J Hazard Mater* 244–245:160–170. doi:[10.1016/j.jhazmat.2012.11.028](https://doi.org/10.1016/j.jhazmat.2012.11.028)
- Zuev VV, Kostromin SV, Bronnikov SV (2008) Nature of the liquid-crystalline phase in supramolecular linear polymers. *Polym Sci Ser B* 50(7–8):177–181. doi:[10.1134/S1560090408070051](https://doi.org/10.1134/S1560090408070051)